

Predicting Radionuclide Release Rates from Spent Nuclear Fuel Inside a Failed Waste Disposal Container Using a Finite Element Model

Nazhen Liu,^{†,***} Ziyang Zhu,^{*} Linda Wu,^{****} Zack Qin,^{*} James J. Noël,^{*****} and David W. Shoesmith^{*****}

Models for the corrosion of spent nuclear fuel (fission and actinide-doped uranium dioxide) provide the essential source term for the release of radionuclides from within a failed nuclear waste container in a deep geologic repository. Although redox conditions within a repository are expected to be anoxic, exposure of the fuel to groundwater will cause the generation of oxidants at the fuel surface, leading to its corrosion and the release of radionuclides. The influence of these oxidants will be partially mitigated by the anoxic corrosion of the inner walls of the steel container to produce the oxidant scavengers, Fe²⁺ and H₂. This review summarizes the development of a finite element model developed to determine the influence of the various redox-controlling species (H₂O₂, Fe²⁺, H₂). Both one-dimensional and two-dimensional models are described, with the latter required to take into account the fractured geometry of the fuel.

KEY WORDS: COMSOL, corrosion, modeling, spent nuclear fuel, uranium dioxide, waste disposal

INTRODUCTION

The universally accepted approach for the safe disposal of spent nuclear fuel is to bury it in a deep geologic repository (DGR). The accepted repository concept is based on multiple barriers, including the fuel waste form, durable metal containers, a clay buffer and seals around the container, and the stable geologic formation, Figure 1. The corrosion resistant container is expected to be a key barrier in this sequence, isolating the fuel from the repository environment. In Canada, Sweden, and Finland, the proposed container comprises a steel vessel, or insert, with an outer barrier layer of copper, in the form of either a shell or a deposited coating.¹

While there is confidence that long-term containment can be achieved, it is judicious to examine the possible consequences of container failure, which could allow contact of the fuel with groundwater. Although anoxic conditions are expected to prevail in a DGR, the radiation fields associated with the fuel waste form could lead to the generation of oxidants by groundwater radiolysis within a failed container. Radiolytically-produced H₂O₂ is expected to be the dominant oxidant,² which can oxidize the insoluble U^{IV} in the UO₂ fuel to the more soluble U^{VI} (as UO₂²⁺), leading to the corrosion of the fuel and the release of radionuclides to the groundwater.²⁻³

Within the failed container, there will be two corrosion fronts: one on the fuel surface driven by the radiolytic oxidants, and a second on the inner surface of the carbon steel vessel or Fe insert, driven by the reduction of H₂O. The redox condition within

the container will be inevitably influenced by the soluble Fe²⁺ and H₂, produced by the second corrosion process,⁴⁻⁶ Figure 2. As illustrated in the figure, the redox coupling of the two corrosion fronts could potentially lead to the scavenging of the radiolytic oxidants and a suppression of the fuel corrosion/radionuclide release processes.

A considerable experimental effort to acquire the databases required to develop models to predict the fuel corrosion process has been undergone, and reviews have been published.⁷⁻⁸ Of these models, three have attempted to account for the influence on fuel corrosion of the evolution of redox conditions with time inside a failed container.⁹⁻¹¹ Two of the three models⁹⁻¹⁰ are one-dimensional electrochemical reaction/diffusion models based on mixed potential theory, which enables them to predict the evolution of the fuel corrosion potential and corrosion current as the radiation fields within the fuel decay with time. The third model is a chemical reaction/diffusion model originally developed in one-dimensional (1D) form,¹¹ but recently extended to two-dimensional (2D) form.¹² The 2D model takes into account the complex geometry of spent fuel, in particular, the extensive fracturing that occurs due to the stress from thermal tension during in-reactor irradiation and during the cooling that occurs on removal of the fuel from the reactor.¹³ These fractures provide primary pathways for groundwater access to deep locations within the fuel, where the scavenging of radiolytic oxidants by the products of steel corrosion could be limited.

Submitted for publication: May 5, 2018. Revised and accepted: June 22, 2018. Preprint available online: June 22, 2018, <https://doi.org/10.5006/2866>.

[†] Corresponding author. E-mail: nliu63@uwo.ca.

^{*} Department of Chemistry, The University of Western Ontario, London, Ontario N6A 5B7, Canada.

^{**} Key Laboratory of Marine Environmental Corrosion and Bio-fouling, Institute of Oceanology, Chinese Academy of Sciences, Qingdao 266071, China.

^{***} Canadian Nuclear Laboratories, Chalk River, Ontario K0J 1J0, Canada.

^{****} Surface Science Western, The University of Western Ontario, London, Ontario N6G 0J3, Canada.

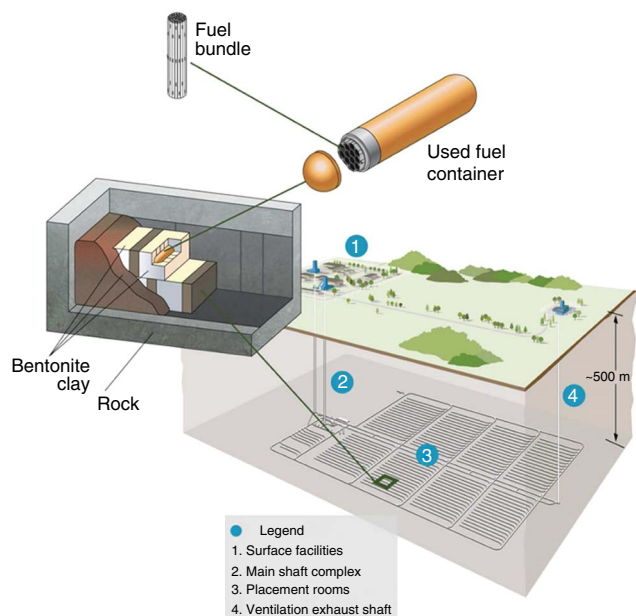


FIGURE 1. Schematic representation of the proposed Canadian deep geologic repository illustrating the multiple barrier approach to disposal.

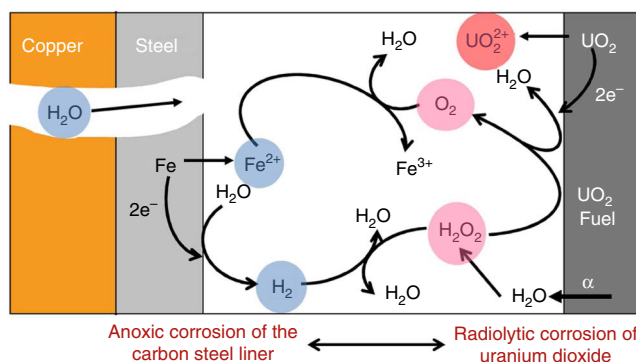


FIGURE 2. Schematic illustration showing the key redox controlling reactions inside a failed waste container.

This review summarizes the progress made on the development of this last model. The emphasis is placed on evaluating how the various processes possible within a failed container will influence the redox conditions at the fuel surface, and hence, the corrosion behavior of the fuel.

MODEL DESCRIPTION

2.1 | Essential Spent Fuel Properties

The universally common form of nuclear fuel is stoichiometric UO_2 , fabricated as high density (94% to 97% of theoretical) ceramic pellets and contained within Zircaloy[†] sheathing. The basic chemical and physical properties of UO_2 have been summarized.¹⁴ While the solubility of UO_2 is extremely limited,¹⁵ it increases substantially under oxidizing conditions, making the stability of fuel strongly dependent on the redox conditions to which it is exposed.

The chemical changes to the fuel induced by in-reactor irradiation have been described elsewhere.⁴ The fuel can be

[†] Trade name.

considered to be a rare-earth (RE^{III})-doped UO_2 matrix containing segregated noble metal (ϵ) particles.¹⁶ Both the extent of RE^{III} -doping and the number density of ϵ -particles increase with the extent of fuel burn-up, leading to the improvement of the electrical conductivity of the fuel matrix. From the corrosion perspective, the fuel can be considered a conductive/reactive matrix containing noble metal (Pd, Ru, Rh, Mo) particles, which can act as either anodes or cathodes, depending on the prevailing redox conditions.

2.2 | Model Reactions

Figure 3 shows the main reactions involved in controlling the redox conditions, and hence, the process of fuel corrosion. This reaction scheme has been established based on extensive international experimental programs. The model includes the following reactions:

- (i) The production of H_2O_2 and H_2 by H_2O radiolysis (1).
- (ii) The corrosion of UO_2 supported by the reduction of H_2O_2 on the UO_2 surface (2a) and on ϵ -particles (2b).
- (iii) The reduction of oxidized surface species (U^{V} and U^{VI}) by H_2 oxidation on ϵ -particles (3a); of dissolved UO_2^{2+} by H_2 in solution (3b); and of adsorbed UO_2^{2+} by H_2 activated on ϵ -particles (3c).
- (iv) The consumption of H_2O_2 by reaction with soluble Fe^{2+} (4).
- (v) Surface reaction between H_2O_2 and H_2 , catalyzed by ϵ -particles (5).
- (vi) The decomposition of H_2O_2 to O_2 and H_2O at the UO_{2+x} surface (6).

The kinetics of these reactions have been discussed in detail elsewhere.^{12,16} It is assumed that groundwater contains a sufficient $\text{HCO}_3^-/\text{CO}_3^{2-}$ to completely complex and dissolve the corrosion products in the form of $\text{UO}_2(\text{HCO}_3)_2^{2-a}$; as a result, no corrosion products would deposit on the surface to impede the dissolution of the waste form as UO_2^{2+} . The rates of the various reactions are described by a series of 1D reaction-diffusion equations. The mathematical model is numerically solved using COMSOL Multiphysics[†], based on the finite element method using the chemical engineering and dilute species transport modules. The values of the parameters used in calculations have been listed and discussed in detail elsewhere.^{11-12,17}

2.3 | Radiolysis Model

Only α -radiolysis is considered as a source of oxidants, as it is reasonable to assume that containment will be maintained for the few hundred years required for γ/β radiation fields to decay to innocuous levels, Figure 4.¹⁸ The dose rate is non-uniformly distributed along the very short penetration pathway of α -particles. Despite this feature, the model assumes a uniform distribution within a radiation zone of 13 μm at the fuel/ H_2O interface, as illustrated in Figure 5.¹⁹ The basis for the adoption of such a layer has been discussed previously.¹¹ The consequences of this assumption have been analyzed¹¹ and shown to have only a marginal effect on model calculations.

Only the molecular species, H_2O_2 and H_2 , are used in calculations, despite radiolysis measurements and models demonstrating the formation of a wide spectrum of radical species. This approximation is justified because the steady-state concentrations of radicals generated by continuous α -radiolysis are 2 to 5 orders of magnitude lower than those of the stable molecular products. Compared to the model calculations based on a full set of α -radiolysis reactions (i.e., including

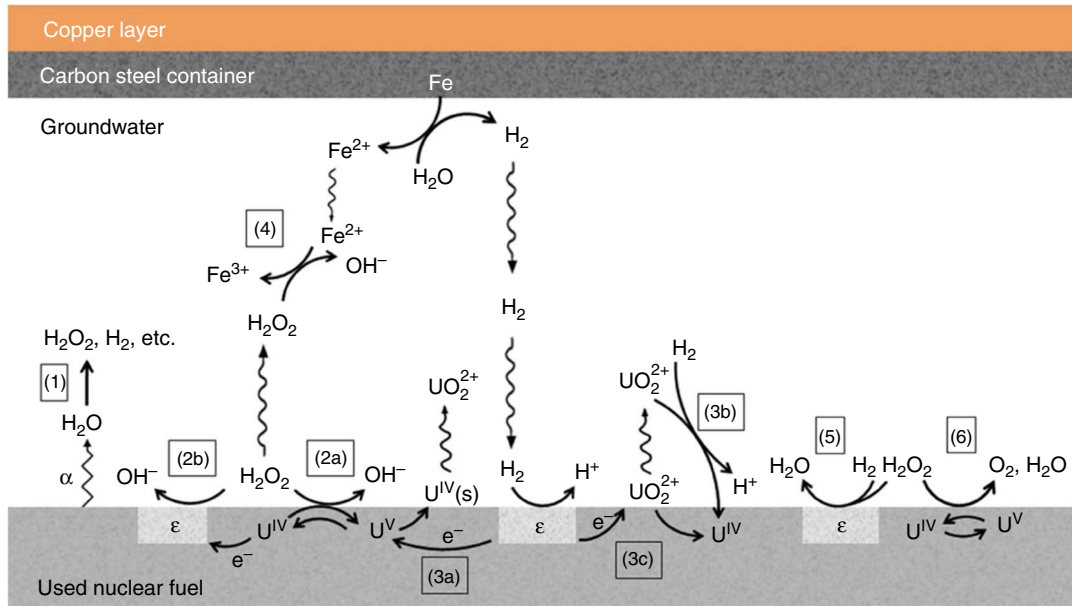


FIGURE 3. Schematic illustration of the reactions included in the model for the α -radiolytic corrosion of spent nuclear fuel.

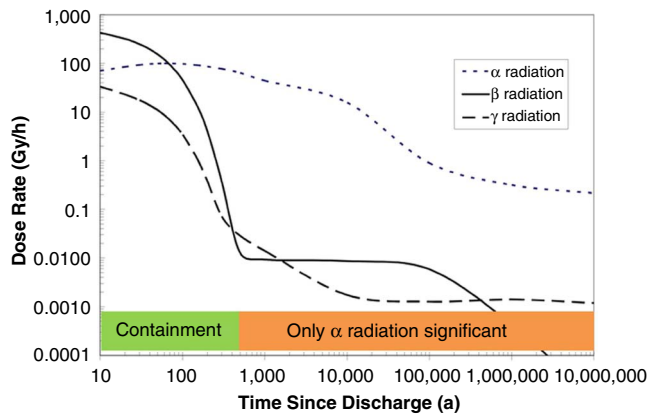


FIGURE 4. α , β , and γ radiation dose rates as a function of time for a layer of water in contact with a CANDU fuel bundle with a burn-up of 220 MWh/kgU.

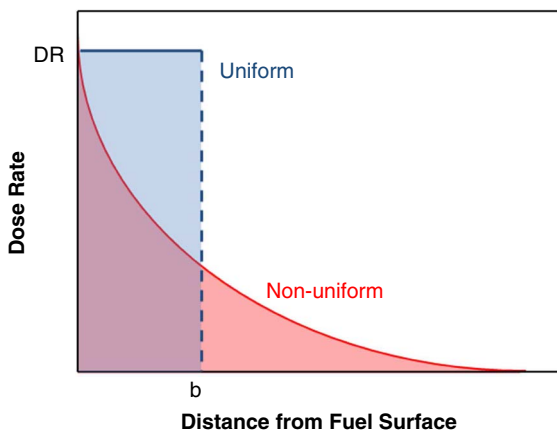


FIGURE 5. Illustration showing the two different dose rate distributions, uniform and exponential. The colored areas indicate the total dose rate in each case.

those involving radical production), the calculations based on the simplified model (only including H_2O_2 and H_2 production) show an overestimate of $[H_2O_2]$ by 21% and of $[H_2]$ by $\sim 3\%$. The reasons for the overestimation of $[H_2O_2]$ could be: (1) the modification of the G-value for H_2O_2 from 0.104 $\mu\text{mol}/\text{J}$ to 0.1248 $\mu\text{mol}/\text{J}$; or (2) the radicals produced will effectively recombine to yield H_2O_2 ($2OH\cdot \rightarrow H_2O_2$; $H\cdot + HO_2\cdot \rightarrow H_2O_2$). This overestimation leads to an increased $[UO_2^{2+}]$ by a conservative 20%.¹⁷ Model calculations are performed using an average α dose rate at the fuel surface of $9.03 \times 10^5 \text{ Gy a}^{-1}$,¹⁹ calculated for a typical CANDU fuel bundle with a burn-up of 220 MWh/kgU at 1,000 y after discharge from reactor.

ONE-DIMENSIONAL (1D) AND TWO-DIMENSIONAL (2D) MODELS

3.1 | One-Dimensional (1D) Model

Figure 6 shows the characteristics of the fuel/groundwater interface, with x indicating the distance from the fuel surface, and b the thickness of the uniform radiation zone. The diffusion layer is the distance over which species can diffuse to, and from, the fuel surface, and beyond which uniform concentrations of all species are presumed to prevail. The length of this layer can be taken to represent the distance of the spent fuel surface from a flaw in the cladding, beyond which the concentrations of Fe^{2+} and H_2 ($[H_2]_{\text{bulk}}$) generated by carbon steel corrosion are constant (i.e., a constant corrosion rate of the steel is assumed) and the concentrations of species produced at the fuel surface (i.e., H_2O_2 and UO_2^{2+}) reach zero. This allows the $[Fe^{2+}]$ and $[H_2]$ adopted to represent different steel corrosion rates without the need to incorporate a specific corrosion model.

The efficacy and validity of adopting such an approach has been evaluated. Model sensitivity calculations showed that varying the diffusion length over 3 orders of magnitude caused only a change in fuel corrosion rate of a factor of 2. In addition, a combined experimental/modeling study was undertaken²⁰ to investigate the possibility of passivation of the steel surface inside a failed waste container. In the experimental part, the corrosion of carbon steel was studied by adding small

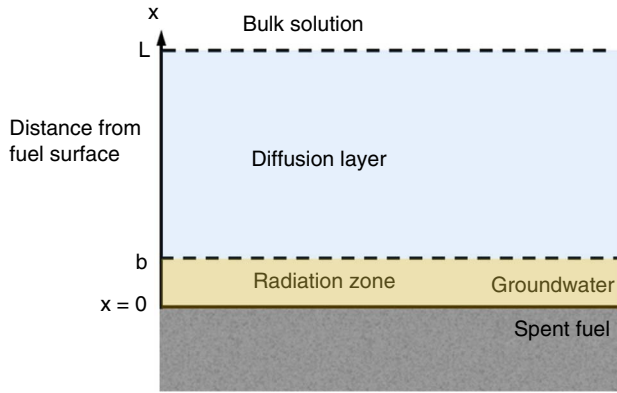


FIGURE 6. Illustration of the 1D α -radiolysis model.

concentrations of H_2O_2 . By adapting a previously developed 1D model¹² for fuel and steel corrosion, calculations were performed to simulate the $[H_2O_2]$ expected on the inside surface of the steel. The adapted model takes account of the long-term corrosion rate of steel under anaerobic conditions (around 0.1 $\mu\text{m/y}$). This study demonstrated that radiolytically-produced oxidants (i.e., H_2O_2) could not achieve sufficiently high concentrations at the steel surface to induce passivation, thereby suppressing the steel corrosion rate and inhibiting the supply of the radiolytic scavengers, Fe^{2+} and H_2 .

3.2 | Two-Dimensional (2D) Model

As spent fuel is heavily fractured and possesses a large number of fission gas bubbles/tunnels, especially along grain boundaries, there is the possibility that the groundwater will penetrate deep within the fuel, leading to the local accumulation of radiolytic species at locations inaccessible to the oxidant scavengers from steel corrosion. To investigate the potential consequences of such physical features, the model was extended to 2D. The 2D arrangement adopted is illustrated in Figure 7. A simplified rectangular geometry is adopted for the cross-sectional area and the dimensions of a fracture determined by its width and depth. α -particle emission is assumed to occur uniformly across the surface, which can be considered wrapped in a thin radiation zone. The diffusion zone, defined above, is retained. In this geometric arrangement, the dose rate is uniformly distributed except at the deep corners of the fracture, where it will be doubled, and at the top of the fracture, where it will be reduced.

THE INFLUENCE OF VARIOUS CHEMICAL AND PHYSICAL FEATURES ON FUEL CORROSION RATES

4.1 | The Influence of Fe^{2+}

The Fe^{2+} ions produced by the anoxic corrosion of steel will undergo the Fenton reaction (Figure 3, Reaction [4]). This reaction is considered irreversible for the pH range anticipated in groundwater ($6 \leq \text{pH} \leq 9$), because the solubility of Fe^{3+} will be $<10^{-8}$ mol/L and 2 to 4 orders of magnitude lower than that of Fe^{2+} .²¹ To account for possible variations in the corrosion rate of the steel, the $[Fe^{2+}]$ was varied over the range 0.01 $\mu\text{mol/L}$ to 1 $\mu\text{mol/L}$ and its influence on H_2O_2 consumption and, hence, the fuel corrosion rate calculated. Figure 8 shows the influence of $[Fe^{2+}]$ on the $[H_2O_2]$ profile from the corroding UO_2 surface to the diffusion layer boundary (set at 1 mm) for the 1D model. For low $[Fe^{2+}]$ (≤ 0.01 $\mu\text{mol/L}$), the consumption of H_2O_2 is minor, the

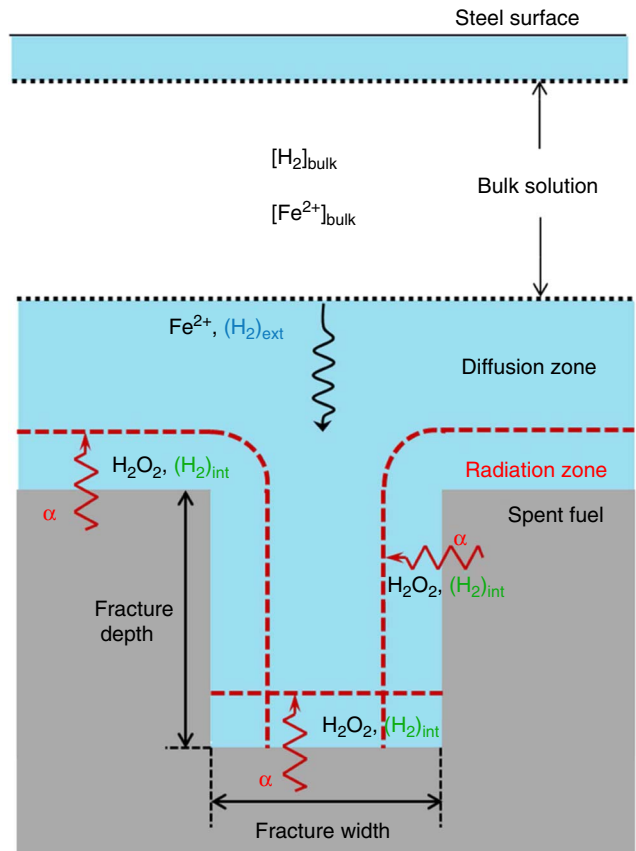


FIGURE 7. Model arrangement showing a cross section of the fuel/solution interface for the simulation of radiolytic corrosion inside a fracture in a fuel pellet. The area in blue indicates the diffusion zone, and the region at the fuel surface within the dashed red line indicates the radiation zone.

surface $[H_2O_2]$ available to drive fuel corrosion being only marginally reduced. However, when the $[Fe^{2+}]$ is increased to values close to the solubility limit for Fe^{2+} (1 $\mu\text{mol/L}$), the surface $[H_2O_2]$ is suppressed to only 10% of its maximum value, showing that this scavenging reaction can significantly reduce the fuel corrosion rate. Calculations using the 2D model show that the influence of $[Fe^{2+}]$ on the fuel corrosion process is overwhelmed within fractures by the influence of H_2 , as will be discussed below.

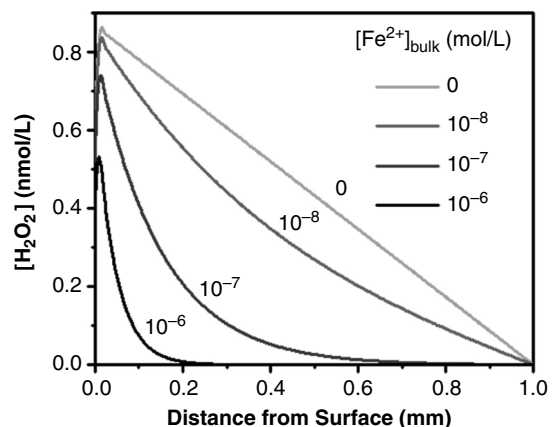


FIGURE 8. The influence of Fe^{2+} (from steel corrosion) on the $[H_2O_2]$ profile at the fuel/solution interface calculated using the 1D model.

4.2 | The Influence of H₂

A considerable effort has been expended on the study of the effect of H₂ because it appears to have the potential to completely suppress fuel corrosion.²²⁻²³ Calculations²² indicate that dissolved [H₂] as high as ~40 mmol/L could be generated as a consequence of steel corrosion in sealed repositories. The key requirement for H₂ to suppress fuel corrosion is that a mechanism be available to activate H₂ by dissociation to produce H• radicals on the fuel surface. A range of studies have shown that this can be achieved by catalysis on ε-particles²³ and by interaction of solutions containing H₂ with either γ or α radiation,²²⁻²³ with the latter path involving the reaction of OH• (an H₂O radiolysis product) and H₂ to produce H• radicals (Wu, et al.,¹⁷ and references therein).

As shown in Figure 3, there are a number of pathways by which H₂ can influence fuel corrosion. The mechanistic and kinetic details of these reactions have been discussed in detail elsewhere.²²⁻²⁶ Besides production by steel corrosion, H₂ will also be generated radiolytically. Calculations using the 1D model showed the influence of radiolytic H₂ production appeared to be minor compared to that produced by steel corrosion. This was demonstrated by sensitivity calculations performed with and without the contribution of radiolytic H₂ in the presence of relatively small [H₂] from steel corrosion (0.01 μmol/L). Ignoring radiolytic H₂ leads to an increase in the fuel corrosion rate by ~10%.

As Fe²⁺ can also suppress the corrosion rate (as discussed above), the amount of H₂ required to completely suppress fuel corrosion (defined as the critical H₂ concentration, [H₂]_{crit}) was calculated with a specified [Fe²⁺]. Figure 9 shows the required [H₂]_{bulk} in the absence of Fe²⁺ as well as over the range of [Fe²⁺] considered above, and demonstrates that, even if the ability of Fe²⁺ to scavenge H₂O₂ is not considered, an [H₂]_{crit} of only ~0.2 μmol/L is required to completely suppress fuel corrosion. This represents a minuscule requirement when compared to the ~40 mmol/L potentially available in a sealed DGR.²²

Within fractures in the fuel, it is possible radiolysis could lead to the accumulation of radiolytic oxidants inaccessible to externally produced reductants, which was investigated using the 2D model. Calculations show that, as the depth of fractures increases, the [H₂] increases significantly while the [H₂O₂] reaches a plateau. Considering that the primary radiolytic yields are the same for the two species in the model, this difference can be attributed to a number of features: (i) the externally supplied H₂; (ii) H₂ is stable whereas H₂O₂ is consumed by its decomposition to yield the much less reactive O₂;²⁷⁻²⁸ and (iii) H₂O₂ and H₂ react with the fuel surface at different rates.¹⁷ This imbalance between [H₂O₂] and [H₂] influences the competition between UO₂ oxidation by H₂O₂ and its reduction by H₂.

In the 2D simulation, the corrosion rate of spent fuel (represented by the diffusive flux of UO₂²⁺ in the direction normal to the surface), Figure 10, reaches a maximum near the mouth of the fracture, and approaches zero at the base of the fracture, the latter indicating a very significant suppression of corrosion. As the access of external reductants, Fe²⁺ and bulk H₂, to deep locations within the fracture is limited, this suppression reflects the accumulation of radiolytic H₂, which is greatest at the base of the fracture.

The variation in corrosion rate along the fracture walls can be attributed to the variations in [H₂O₂] and [H₂], the former remaining constant while the latter increases with depth. As the fracture mouth is approached, the rapid decrease in corrosion rate is attributed to the prompt decrease in [H₂O₂], as it (1) diffuses out of the fracture; and (2) is consumed by the Fe²⁺

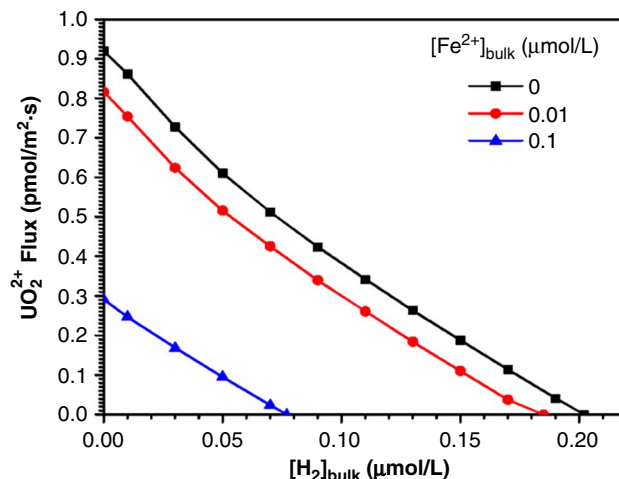


FIGURE 9. Fuel corrosion rate (expressed as the flux of dissolved UO₂²⁺) as a function of the concentration of H₂ from steel corrosion calculated using the 1D model.

diffusing in. By separating the contributions to corrosion suppression by internal (radiolytic) and external (steel corrosion) H₂, the role of the former at deep locations was confirmed.²⁹

To obtain the [H₂]_{crit}, the UO₂²⁺ flux in the direction normal to the fuel surface (equivalent to the corrosion rate) was calculated as a function of [H₂]_{bulk}. The [H₂]_{crit} is taken to be achieved when corrosion is completely suppressed at all surface locations. To simulate the range of fracture geometries anticipated in fractured fuel pellets,¹³ [H₂]_{crit} was calculated for a wide range of fracture depths and widths. Figure 11 shows [H₂]_{crit} increases to a peak value and then decreases as the fracture deepens. Within the fracture dimensions tested, [H₂]_{crit} never exceeds a maximum contribution from external (bulk) H₂ of 2.4 μmol/L, indicated by the dashed line in Figure 11. This value is ~12 times the [H₂]_{crit} required to completely suppress corrosion on a planar surface, demonstrating that, while a larger contribution of H₂ from steel corrosion is required in fractures, the demand is not high.

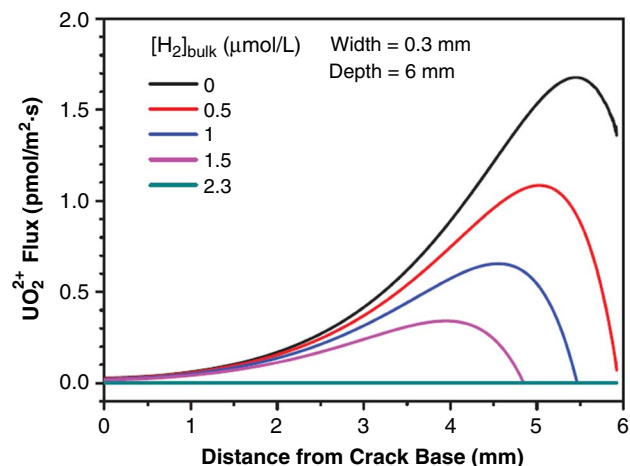


FIGURE 10. The diffusive flux of UO₂²⁺ (the corrosion rate), calculated using the 2D model, in the direction normal to the wall of a fracture, calculated using the 2D model, as a function of the distance from the base of the crack at various concentrations of H₂ provided by steel corrosion.

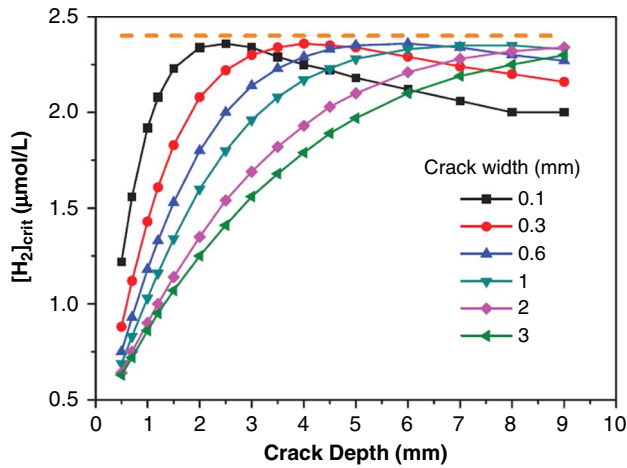


FIGURE 11. The calculated $[H_2O_2]_{crit}$ required to completely suppress fuel corrosion in fractures (cracks) with different widths and depths, $[Fe^{2+}] = 0.01 \mu\text{mol/L}$. The dashed line indicates an upper limit of $2.4 \mu\text{mol/L}$ for $[H_2O_2]_{crit}$.

4.3 | The Influence of H_2O_2 Decomposition

While no complete kinetic understanding of H_2O_2 decomposition (to O_2 and H_2O) has yet been developed, H_2O_2 decomposition will influence the demand for $[H_2]_{bulk}$ to suppress corrosion, although the influence is not expected to be major.¹⁷ Experimental and theoretical calculations on UO_2 and a range of transition metal oxide surfaces show that decomposition proceeds via the formation of $OH\cdot$ radicals.³⁰ By comparing the amount of H_2O_2 consumed to the amount of U dissolved,²⁸ it was shown that H_2O_2 decomposition was the major pathway for its consumption, with the dissolution yield for simulated high-burn-up UO_2 fuel (SIMFUEL) being considerably less (0.2%) than that for pure UO_2 (14%). Recent electrochemical results demonstrate that this can be attributed to stabilization of the UO_2 matrix by fission product (rare earth) doping.³¹⁻³²

Figure 12 shows that the demand for H_2 from steel corrosion ($[H_2]_{crit}$) decreases substantially as the decomposition ratio (the fraction of H_2O_2 decomposed, as opposed to causing corrosion) increases, but increases as the fracture depth increases. As O_2 , an alternative oxidant for UO_2 , is produced by decomposition, the influence of this reaction remains to be fully investigated.

4.4 | Model Validation

An attempt to validate the model has been made by comparing model predictions to a wide range of corrosion rate measurements as a function of α -source strength,³³ Figure 13. These measurements were conducted on a wide range of specimens (α -doped UO_2 , Pu-doped UO_2 , spent fuels, simulated spent fuels, and UO_2) under different exposure conditions. Despite the variability in the values, a clear trend of increasing corrosion rate with increasing α -source strength was established. In Figure 13, three sets of data (marked A, B, and C) cannot be considered to fit the linear relationship. For A, corrosion rates were calculated based on electrochemical impedance spectroscopy measurements, in which large errors due to the high resistance of the materials led to the overestimation of the rates. The value labeled B was measured in a clay environment containing reducing species, leading to unexpectedly low values. The values labeled C were

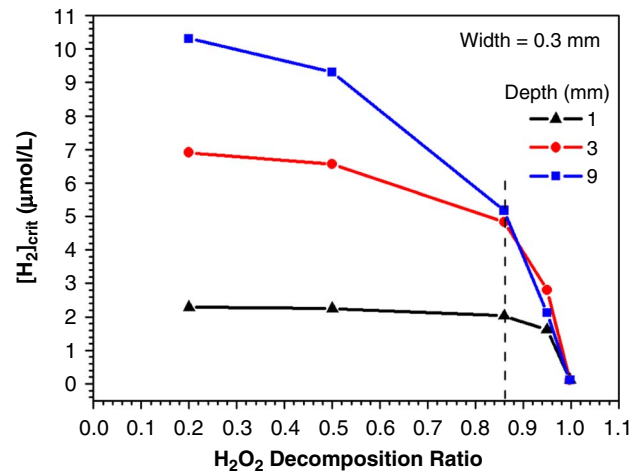


FIGURE 12. The calculated $[H_2O_2]_{crit}$ as a function of the H_2O_2 decomposition ratio and the depth of a fracture. The vertical dashed line shows the default value of H_2O_2 decomposition ratio (0.86). The modified reaction rate constants for Reactions (3c) and (5), from Figure 3, were adopted in the calculation.²⁹

measured on Pu-containing specimens, and it has been suggested that the low rates indicate a stabilizing influence of Pu on the UO_2 matrix.

To appropriately test the model, only measurements performed on α -doped UO_2 (with ^{233}U and ^{238}Pu) were used. As the measurements were normally performed in an oxygen-free environment in an open system, this would allow gases generated directly or indirectly by α -radiolysis, such as O_2 and H_2 , to escape. To account for this, the boundary condition for H_2 and O_2 at the diffusion boundary was set with concentrations equal to zero. In addition, reactions involving ϵ -particles and reactions involving scavengers produced by steel corrosion were also removed.³⁴

Figure 14 compares the model prediction to the experimental values and demonstrates a very good correlation. This agreement, and a series of sensitivity calculations for various model parameters, demonstrate that the dominant factor controlling the corrosion rate is the rate of radiolytic production of

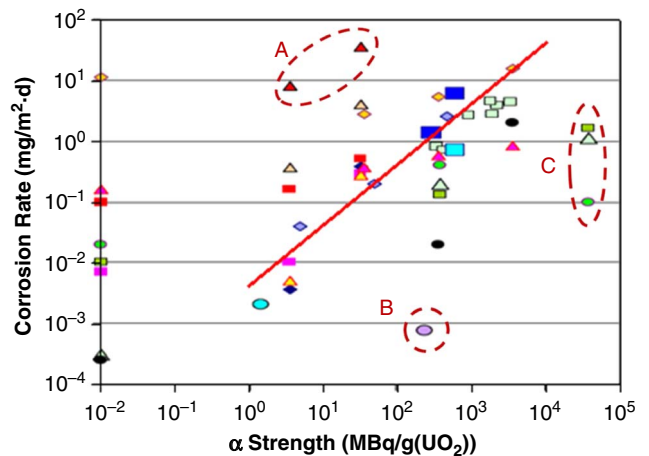


FIGURE 13. Corrosion rates of α emitter-doped UO_2 , non-doped UO_2 (0.01 MBq/g), SIMFUEL, and spent fuel. The red line indicates a linear least squares fit to the data. The values marked A, B, and C are discussed in the text.

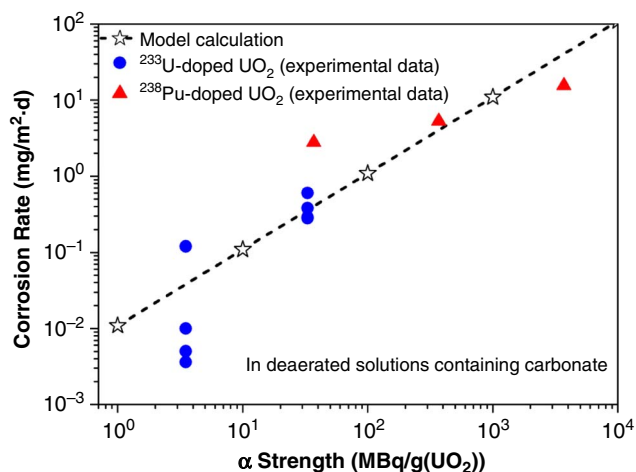


FIGURE 14. Comparison of the calculated corrosion rate to corrosion rates made on α -doped UO_2 specimens.³²

H_2O_2 , which is directly proportional to the α -source strength of the fuel, a feature determined by the extent of in-reactor burn-up.

References

- P.G. Keech, P. Vo, S. Ramamurthy, J. Chen, R. Jacklin, D.W. Shoesmith, *Corros. Sci. Technol.* 49 (2014): p. 425-430.
- E. Ekeröth, O. Roth, M. Jonsson, *J. Nucl. Mater.* 355 (2006): p. 38-46.
- D.W. Shoesmith, *J. Nucl. Mater.* 282 (2000): p. 1-31.
- D.W. Shoesmith, "Used Fuel and Uranium Dissolution Studies—A Review," Nuclear Waste Management Organization, report no. TR-2007-03, 2007.
- D.W. Shoesmith, "The Role of Dissolved Hydrogen on the Corrosion/ Dissolution of Spent Nuclear Fuel," Nuclear Waste Management Organization, report no. TR-2008-19, 2008.
- G.M. Kwong, "Status of Corrosion Studies for Copper Used Fuel Containers Under Low Salinity Conditions," Nuclear Waste Management Organization, report no. TR-2011-14, 2011.
- B. Grambow, J. Bruno, L. Duro, J. Merino, A. Tamayo, C. Martin, G. Pepin, S. Schumacker, O. Smidt, C. Ferry, C. Jegou, J. Quinones, E. Iglesias, N. Rodriguez Villagra, J.M. Nieto, A. Martinez-Esparza, A. Loida, V. Metz, B. Kienzler, G. Bracke, D. Pellegrini, G. Mathieu, V. Wasselin-Trupin, C. Serres, D. Wegen, M. Jonsson, L. Johnson, K. Lemmens, J. Liu, K. Spahiu, E. Ekeröth, I. Casas, J. de Pablo, C. Watson, P. Robinson, D. Hodgkinson, "Model Uncertainty for the Mechanism of Dissolution of Spent Fuel in a Nuclear Waste Repository," European Commission Final Report for MICADO Project, EUR 24597, 2010.
- T.E. Eriksen, D.W. Shoesmith, M. Jonsson, *J. Nucl. Mater.* 420 (2012): p. 409-423.
- D.W. Shoesmith, M. Kolar, F. King, *Corrosion* 59 (2003): p. 802-816.
- J.L. Jordan, K. Frey, W. Ebert, *J. Nucl. Mater.* 462 (2015): p. 135-146.
- L. Wu, Y. Beauregard, Z. Qin, S. Rohani, D.W. Shoesmith, *Corros. Sci.* 61 (2012): p. 83-91.
- L. Wu, N. Liu, Z. Qin, D.W. Shoesmith, *J. Electrochem. Soc.* 161 (2014): p. E3259-E3266.
- K.M. Wasywich, W.H. Hocking, D.W. Shoesmith, P. Taylor, *Nucl. Technol.* 104 (1993): p. 309-329.
- D.W. Shoesmith, S. Sunder, W.H. Hocking, "Electrochemistry of UO_2 Nuclear Fuel," in *Electrochemistry of Novel Materials*, eds. J. Lipkowsky, P.N. Ross (New York, NY: VCH Publishers, 1994).
- I. Grenthe, J. Fuger, R.J. Konings, R.J. Lemire, A.B. Muller, C. Nguyen-Trung, H. Wanner, *Chemical Thermodynamics of Uranium*, eds. H. Wanner, I. Forest (Amsterdam, The Netherlands: North Holland, 1992).
- H. He, M. Broczkowski, K. O'Neil, D. Ofori, O. Semenikhin, D.W. Shoesmith, "Corrosion of Nuclear Fuel (UO_2) Inside a Failed Nuclear Waste Container," Nuclear Waste Management Organization, report no. TR-2012-09, 2012.
- L. Wu, Z. Qin, D.W. Shoesmith, *Corros. Sci.* 84 (2014): p. 85-95.
- F. Garisto, "Fourth Case Study: Features, Events and Processes," Nuclear Waste Management Organization, report no. TR-2012-14, 2012.
- F. Garisto, D.H. Barber, E. Chen, A. Inglot, C.A. Morrison, "Alpha, Beta and Gamma Radiation Dose Rates in Water in Contact with Used CANDU Fuel," Nuclear Waste Management Organization, report no. TR-2009-27, 2009.
- S.L.W. Hill, N. Liu, Z. Qin, D. Zagidulin, D.W. Shoesmith, "Interactions Between Carbon Steel and UO_2 Corrosion Fronts Inside a Failed Nuclear Waste Container," Proceedings of the 17th International Conference on Environmental Degradation of Materials in Nuclear Power Systems—Water Reactors, August 9-12, 2015 (Toronto, Canada: Canadian Nuclear Society, 2015).
- C.F. Baes, R.E. Mesmer, *The Hydrolysis of Cations* (New York, NY: Wiley InterScience, 1976).
- P. Carbol, J. Cobos-Sabate, J.-P. Glatz, C. Ronchi, V. Rondinella, D.H. WEgen, T. Wiss, A. Loida, V. Metz, B. Kienzler, K. Spahiu, B. Grambow, J. Quinones, A. Martinez Esparza Valiente, "The Effect of Dissolved Hydrogen on the Dissolution of ^{233}U -doped UO_2 , High Burn-up Spent Fuel and MOX Fuel," Swedish Nuclear Fuel and Waste Management Company, report no. TR-05-09, 2005.
- M.E. Broczkowski, D. Zagidulin, D.W. Shoesmith, "The Role of Dissolved Hydrogen on the Corrosion/Dissolution of Spent Nuclear Fuel," Nuclear Energy and the Environment, American Chemical Society Symposium (Washington, DC: ACS, 2010), p. 349-380.
- E. Ekeröth, M. Jonsson, T.E. Eriksen, K. Ljungqvist, S. Kovacs, I. Puigdomenech, *J. Nucl. Mater.* 334 (2004): p. 35-39.
- S. Nilsson, M. Jonsson, *J. Nucl. Mater.* 372 (2008): p. 160-163.
- S. Nilsson, M. Jonsson, *J. Nucl. Mater.* 374 (2008): p. 290-292.
- M. Lousada, M. Trummer, M. Jonsson, *J. Nucl. Mater.* 434 (2013): p. 434-439.
- R. Pehrman, M. Trummer, C.M. Lousada, M. Jonsson, *J. Nucl. Mater.* 430 (2012): p. 6-11.
- N. Liu, L. Wu, Z. Qin, D.W. Shoesmith, *Environ. Sci. Technol.* 50 (2016): p. 12348-12355.
- C.M. Lousada, A.J. Johansson, T. Brinck, M. Jonsson, *J. Phys. Chem. C* 116 (2012): p. 9533-9543.
- M. Razdan, D.W. Shoesmith, *J. Electrochem. Soc.* 161 (2014): p. H105-H113.
- N. Liu, H. He, J.J. Noël, D.W. Shoesmith, *Electrochim. Acta* 235 (2017): p. 654-663.
- C. Poinssot, C. Ferry, M. Kelm, B. Grambow, A. Martinez, L. Johnson, Z. Andriambololona, J. Bruno, C. Cachoir, J.M. Cavedon, H. Christensen, C. Corbel, C. Jegou, K. Lemmens, A. Loida, P. Lovera, F. Miserque, J. de Pablo, A. Poulesquen, J. Quinones, V. Rondinella, K. Spahiu, D.H. Wegen, "Spent Fuel Stability Under Repository Conditions—Final Report of the European Project," European Commission Report, report no. CEA-R-6093, 2005.
- N. Liu, Z. Qin, J.J. Noël, D.W. Shoesmith, *J. Nucl. Mater.* 494 (2017): p. 87-94.